

Chiral phase transition in a planar four-Fermi model in a tilted magnetic field

Rudnei O. Ramos^{1,*} and Patrícia H. A. Manso^{1,†}

¹*Departamento de Física Teórica, Universidade do Estado do Rio de Janeiro, 20550-013 Rio de Janeiro, RJ, Brazil*

We study a planar four-Fermi Gross-Neveu model in the presence of a tilted magnetic field, with components parallel and perpendicular to the system's plane. We determine how this combination of magnetic field components, when applied simultaneously, affects the phase diagram of the model. It is shown that each component of the magnetic field causes a competing effect on the chiral symmetry in these fermionic systems. While the perpendicular component of the magnetic field tends to make the chiral symmetry breaking stronger, the effect of the parallel component of the field in these planar systems is to weaken the chiral symmetry through the enhancement of the Zeeman energy term. We show that this competing effect, when combined also with temperature and chemical potential, can lead to a rich phase diagram, with the emergence of multiple critical points and reentrant phase transitions. We also study how the presence of these multiple critical points and reentrant phases can manifest in the quantum Hall effect. Our results provide a possible way to probe experimentally chiral symmetry breaking and the corresponding emergence of a gap (i.e., the presence of a nonvanishing chiral vacuum expectation value) in planar condensed matter systems of current interest.

PACS numbers: 11.10.Kk, 71.30.+h, 11.30.Qc

I. INTRODUCTION

The interaction of fermions with an external magnetic field is expected to be associated with phenomena like metal-to-insulating phase transitions in semiconductors [1], the quantum Hall effect [2] and transport properties in superconductors [3], just to mention a few examples in the context of condensed matter physics. Among these systems, planar ones are of particular interest and they include, for example, high-temperature superconductors, organic thin films and most recently, the physics of graphene [4]. Most of these systems have an excitation spectrum that can be well described by relativistic Dirac-like fermions. A typical example is the physics of graphene, in which electron transport is essentially governed by the Dirac's relativistic equation. It is then expected that these types of planar systems can be appropriately described by quantum field theory models in two spatial dimensions. In this context, the Gross-Neveu (GN) type of models [5] in $2 + 1$ dimensions are very popular not only because of their simplicity, but also for their ability to capture many of the relevant physics exhibited by planar fermionic systems in general. These models can have either a discrete, $\psi \rightarrow \gamma_5 \psi$, or a continuous, $\psi \rightarrow \exp(i\alpha\gamma_5)\psi$, chiral symmetry. They consist of N massless four-component fermions self-interacting through a local four-Fermi interaction.

One of the most basic motivations for studying the properties of fermionic planar systems is to determine whether we can have a metal-to-insulating type of transition under the variation of external parameters, like temperature, chemical potential and external fields, e.g., an external magnetic field. The metal-insulator transition is directly connected to the presence of a nonvanishing gap in the excitation spectrum for the fermions and how this gap eventually vanishes in the presence of external conditions. In the quantum field theory context, a mass term for the fermions can be generated dynamically in the absence of external conditions, like in the original GN model, and it is associated with the breaking of the chiral symmetry in the model.

In this work we make use of the original GN model with discrete chiral symmetry and study the chiral phase transition when the system is in the presence of an external tilted magnetic field, i.e., a magnetic field that includes both parallel and perpendicular components that are being applied simultaneously to the system (see Fig. 1). This model has been previously extensively analyzed when in the presence of a magnetic field applied perpendicular to the plane (see, for example, Refs. [6, 7] for some of the earlier studies) and, more recently, in the presence of an in-plane magnetic field [8]. But, surprisingly, a study of both types of fields, parallel and perpendicular to the system's plane, applied simultaneously is still lacking. Perhaps the reason for this negligence in the literature was because not much was expected for the effects on the system symmetry due to a parallel component of the field. However, there are good reasons for making this study. It is well known that a perpendicular magnetic field B_\perp leads to an *enhancement* of

*Electronic address: rudnei@uerj.br

†Electronic address: phmansophy@gmail.com

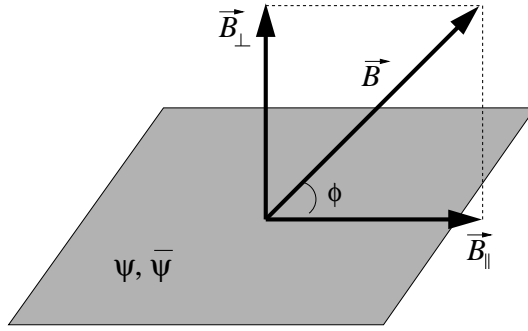


FIG. 1: A schematic representation of the system under study, consisting of fermions in a plane and in the presence of a magnetic field \vec{B} that makes an angle ϕ with respect to the plane.

the chiral-symmetry-broken region (thus, it tends to increase a gap in the excitation spectrum). This is the magnetic catalysis phenomenon that can occur for all values of the four-Fermi interaction strength [6, 7]. However, an in-plane magnetic field B_{\parallel} has been shown to produce an opposite effect [8], leading to a *reduction* of the chiral symmetry broken region. In other words, a parallel component of the magnetic field tends to act on restoring the chiral symmetry for large enough values of B_{\parallel} . This is due to the fact that the in-plane magnetic field contributes to enhance the Zeeman energy term (which depends on the total magnetic field applied to the system), which in turn leads to larger effective polarization of the system. The polarized planar fermionic system tends to exhibit less chiral symmetry.

Since the application of perpendicular and parallel (in-plane) magnetic fields leads to opposite effects on the chiral symmetry, it is reasonable to expect the combination of both components, when applied simultaneously to the system, to possibly lead to new patterns for the chiral phase transition. We will show in this work that this indeed can happen under an appropriate choice of parameters. In this paper we show that the application of both B_{\perp} and B_{\parallel} , with the combined effects of temperature T and chemical potential μ , can lead to a phase diagram that can display a rich structure, with the possibility of exhibiting multiple critical points and reentrant phases. We show that this is a consequence of the competing effects on the system's chiral symmetry coming from each component of the applied oblique external magnetic field.

This paper is organized as follows: In Sec. II we briefly revise the four-Fermi GN model used in this work. In Sec. III the thermodynamic effective potential for the fermionic scalar condensate $\langle \bar{\psi}\psi \rangle$ is derived in the mean field theory approximation, and results for the phase diagram for the model are displayed. In Sec. IV we study in particular the quantum phase transitions in the model and derive the Hall conductivity. We also discuss the impact that the presence of the possible multiple critical points can have on the Hall conductivity, pointing out a possible way for characterizing experimentally the presence of quantum critical points. Finally, in Sec. V, we give our conclusions and discuss possible applications and extensions of this work.

II. THE FOUR-FERMI MODEL IN THE PRESENCE OF AN EXTERNAL MAGNETIC FIELD

We work with a four-Fermi model, in $2 + 1$ dimensions, of the GN type and with N flavors, described by the Lagrangian density [5]

$$\mathcal{L} = \sum_{s=\uparrow,\downarrow} \sum_{j=1}^N \left[\bar{\psi}_j^s (i \not{\partial}) \psi_j^s + \frac{\lambda}{2N} (\bar{\psi}_j^s \psi_j^s)^2 \right], \quad (2.1)$$

where λ is the coupling and $\not{\partial} \equiv \gamma^{\nu} \partial_{\nu}$, $\nu = 0, 1, 2$, with the gamma matrices being 4×4 matrices, where here we follow the representation given, e.g., in Ref. [9] for fermions in 2+1 dimensions. The model of Eq. (2.1) possesses a discrete chiral symmetry, $\psi \rightarrow \gamma_5 \psi$, $\bar{\psi} \rightarrow -\bar{\psi} \gamma_5$, with the γ_5 matrix defined as in Ref. [9]. This discrete chiral symmetry is the one considered in this paper, along with its breaking and restoration conditions. The chiral symmetry is broken when a gap (a mass term for the fermions) is generated. Since the gap corresponds to a nonvanishing vacuum expectation value for the chiral operator, $\langle \bar{\psi}\psi \rangle$, it is then convenient to rewrite Eq. (2.1) in terms of an auxiliary scalar field σ ,

$$\mathcal{L}[\bar{\psi}, \psi, \sigma] = \sum_{s=\uparrow,\downarrow} \sum_{j=1}^N \bar{\psi}_j^s (i \not{\partial} - \sigma) \psi_j^s - \frac{N}{2\lambda} \sigma^2, \quad (2.2)$$

where σ and the chiral operator are related, from the saddle-point solution for σ , by $\sigma = -(\lambda/N)\bar{\psi}\psi$, with implicit sums over the spin and flavor. In terms of the Lagrangian density (2.2), the discrete chiral symmetry is now expressed as $\psi \rightarrow \gamma_5\psi$, $\bar{\psi} \rightarrow -\bar{\psi}\gamma_5$ and $\sigma \rightarrow -\sigma$.

With the Lagrangian density of Eq. (2.2) expressed in terms of the auxiliary scalar field, it becomes relatively simpler to study the phase diagram of the model, which can be made through the study of the behavior of the vacuum expectation value of σ as a function of the temperature, the chemical potential and the external magnetic field. This study can be made by evaluating the effective potential, or Landau's free energy density, for a constant (background) configuration for the auxiliary scalar field, $V_{\text{eff}}(\sigma_c)$. The effective potential can be obtained by integrating out the fermion fields and fluctuations around the scalar background field [9]. From the effective potential, all the thermodynamics for the model can be derived. In particular, a chiral phase transition is signaled by a nonvanishing vacuum expectation value for σ , $\bar{\sigma}_c \equiv \langle \sigma \rangle$, which is a (global) minimum of $V_{\text{eff}}(\sigma_c)$. Both temperature and chemical potential are introduced through the grand canonical partition function definition,

$$Z(\beta, \mu) = \text{Tr} \exp [-\beta (H - \mu Q)] , \quad (2.3)$$

where β is the inverse of the temperature¹, μ is the chemical potential, H is the Hamiltonian corresponding to Eq. (2.2) and $Q = \int d^2x \bar{\psi}\gamma_0\psi$ is the conserved charge. Furthermore, we can also study the effect of an external magnetic field applied to the system by coupling it to the fermions in Eq. (2.2) in the usual way. For an arbitrary external magnetic field that can have components both parallel and perpendicular to the system's plane, the perpendicular component of the field couples to the fermions orbital motion, generating the Landau levels for fermions in a magnetic field [6, 7], while the total component of the field contributes to an intrinsic Zeeman effect [10]. The effective potential, or free energy density, is defined as usual from the grand canonical partition function Eq. (2.3) by

$$V_{\text{eff}} = -\frac{1}{\beta\mathcal{V}} \ln Z , \quad (2.4)$$

where \mathcal{V} is the volume (or, more specifically, the area in the present problem of a planar system).

Transforming Eq. (2.3) in the form of a path integral, in the imaginary-time (Euclidean) formalism of finite temperature field theory [11], one obtains

$$Z = \int D\sigma \prod_s D\psi^\dagger D\psi \exp \{ -S_E[\bar{\psi}, \psi, \sigma] \} , \quad (2.5)$$

where the functional integration is performed over the fermion fields satisfying the antiperiodic boundary condition in Euclidean time: $\psi_j(x, \tau) = -\psi_j(x, \tau + \beta)$, while over the σ it satisfies periodic boundary conditions. The Euclidean action $S_E[\bar{\psi}, \psi]$ in Eq. (2.5), from the Lagrangian density of Eq. (2.2) in the presence of an external magnetic field with components B_\perp and B_\parallel , perpendicular and parallel to the plane, respectively, is given by²

$$S_E[\bar{\psi}, \psi, \sigma] = \int_0^\beta d\tau \int d^2x \left\{ \sum_{s=\uparrow, \downarrow} \sum_{j=1}^N \bar{\psi}_j^s [\gamma_0 \partial_\tau + i\gamma_1 (\partial_x + ie A_x) + i\hbar\gamma_2 (\partial_y + ie A_y) \right. \\ \left. + \sigma + \gamma_0 \mu + \frac{\sigma_s}{2} \gamma_0 g \mu_B B] \psi_j^s + \frac{N}{2\lambda} \sigma^2 \right\} , \quad (2.6)$$

where A_x and A_y are the external electromagnetic vector potential components, $\sigma_s \gamma_0 g \mu_B B/2$, with $B \equiv |\vec{B}| = \sqrt{B_\perp^2 + B_\parallel^2}$, is the corresponding Zeeman energy term; $\sigma_\uparrow = 1$, $\sigma_\downarrow = -1$; g is the spectroscopic Lande factor and μ_B is the Bohr magneton, $\mu_B = e^2/(2m_e)$. By choosing a gauge where the three-dimensional vector potential is given, for example, by $\vec{A} = (0, B_\perp x, B_\parallel y)$, we see from Eq. (2.6) that B_\perp couples only to the orbital motion of the fermions and

¹ Throughout this work, we assume the natural units $k_B = \hbar = c = 1$.

² Note that in condensed matter systems there should also be a Fermi velocity v_F factor multiplying the space components of the gamma matrices and the coupling constant λ in this expression [8]. (For example, in graphene $v_F \approx c/300$). v_F is omitted in all our expressions, but we will reestablished it when making estimates in the context of condensed matter systems later on.

will result in the Landau levels for the system in this magnetic field. The Zeeman energy term in Eq. (2.6) involves the total magnitude of the magnetic field and originates from the standard form for the Zeeman term as employed in quantum many-body theory, for instance [10]. Note also that from the form of the Zeeman energy term in Eq. (2.6), we see that it can be added to the chemical potential. Thus, in the action S_E , we can define an effective chemical potential term of the form,

$$\begin{aligned} \sum_{s=\uparrow,\downarrow} \sum_{j=1}^N \mu_s \bar{\psi}_j^s \gamma_0 \psi_j^s &= \sum_{s=\uparrow,\downarrow} \sum_{j=1}^N \left(\mu + \frac{\sigma_s}{2} g \mu_B B \right) \bar{\psi}_j^s \gamma_0 \psi_j^s \\ &= \mu_{\uparrow} \psi^{\uparrow\dagger} \psi^{\uparrow} + \mu_{\downarrow} \psi^{\downarrow\dagger} \psi^{\downarrow}, \end{aligned} \quad (2.7)$$

where $\mu_{\uparrow} = \mu + \delta\mu$ and $\mu_{\downarrow} = \mu - \delta\mu$, with $\delta\mu = g \mu_B B/2$. The effect of the total amplitude of the magnetic field is then felt through the asymmetry term $\delta\mu$ in the chemical potential for spin up and spin down, resulting in a polarization of the system. Note that in the language of condensed matter systems, the magnetic field produces the analogue of an asymmetrical doping, or an imbalance between the chemical potentials of the fermions (electrons) with the two possible spin orientations. This asymmetry can be produced by a doping process that alters the densities of spin up and spin down. Physically, the chemical potential μ can be interpreted as to account for the extra density of electrons that is supplied to the system by the dopants, while $\delta\mu$ measures the amount of asymmetry introduced. We should also note that even in the absence of the parallel component of the magnetic field, $B_{\parallel} = 0$, there is still a Zeeman energy term, which is then proportional only to B_{\perp} . However, in most practical applications this Zeeman energy contribution, when compared with the lowest Landau energy level, $\sqrt{2|eB_{\perp}|}$, is very small and can safely be neglected (see the discussion later on in the Conclusions section). The Zeeman energy term is then, e.g. in practical physical systems found in condensed matter systems, only appreciable when $B_{\parallel} \gg B_{\perp}$. Expressing the Zeeman energy term in terms of the tilt angle ϕ of the magnetic field (see Fig. 1), $\delta\mu = g \mu_B B/2 = g \mu_B B_{\parallel} \sqrt{1 + \tan^2 \phi}/2$, we see that the importance of the Zeeman energy term will in general be when $\phi \ll 1$, or $\delta\mu \approx g \mu_B B_{\parallel}/2$, corresponding to a highly tilted magnetic field³. Under these circumstances, the polarization produced by the Zeeman energy term then becomes proportional to B_{\parallel} .

In the analysis we will perform in the following sections on the effect of the magnetic field on the phase structure of the GN model, we will work with the magnetic fields expressed in terms of their contributions through the Landau energy levels (given in terms of B_{\perp}) and in terms of the asymmetry $\delta\mu = g \mu_B B_{\parallel} \sqrt{1 + \tan^2 \phi}/2$. We also keep in mind that for typical physical problems of relevance in condensed matter systems, in order for the asymmetry (Zeeman term) to be strong enough such that it cannot be neglected (when compared with the magnitude of the Landau energy terms), it is required in general that $B_{\parallel} \gg B_{\perp}$, or, equivalently, $\phi \ll 1$, which corresponds to a highly tilted magnetic field (this is also discussed in more detail in the Conclusions section).

III. EFFECTIVE POTENTIAL AND PHASE STRUCTURE

All the thermodynamics, magnetic properties and phase structure of the model Eq. (2.2), as a function of temperature, chemical potential and magnetic field, can be determined from the effective potential Eq. (2.4). It is useful to start by briefly reviewing the derivation of the effective potential and its main results for the GN model, including at first only temperature and chemical potential and then later also including the external magnetic field.

A. The effective potential and phase structure at finite T and μ

From the grand canonical partition function Eq. (2.5), with the action (2.6) (considering it initially in the absence of an external magnetic field), for a constant background scalar field $\langle \sigma \rangle = \sigma_c$, in the mean field approximation, or equivalently, from the leading term in a $1/N$ expansion, or the large- N approximation [12, 13], we obtain that the effective potential V_{eff} for σ_c , at finite T and μ , is given by

³ Alternatively, instead of a highly tilted magnetic field, we could also think in a physical situation where B_{\perp} and B_{\parallel} are generated independently and such that $B_{\parallel} \gg B_{\perp}$.

$$V_{\text{eff}}(\sigma_c, T, \mu) = \frac{N}{2\lambda} \sigma_c^2 - 2NT \sum_{n=-\infty}^{+\infty} \int \frac{d^2 p}{(2\pi)^2} \ln \left[(\omega_n - i\mu)^2 + \mathbf{p}^2 + \sigma_c^2 \right] , \quad (3.1)$$

where $\omega_n = (2n+1)\pi T$ are the Matsubara frequencies for fermions. Performing the sum over the Matsubara frequencies in Eq. (3.1), we find

$$V_{\text{eff}}(\sigma_c, T, \mu) = \frac{N}{2\lambda} \sigma_c^2 - 2N \int \frac{d^2 p}{(2\pi)^2} E_p \quad (3.2)$$

$$- 2NT \int \frac{d^2 p}{(2\pi)^2} \left[\ln \left(1 + e^{-\beta E^+} \right) + \ln \left(1 + e^{-\beta E^-} \right) \right] , \quad (3.3)$$

where $E^\pm = E_p \pm \mu$ and $E_p = \sqrt{\mathbf{p}^2 + \sigma_c^2}$.

At zero temperature and chemical potential the effective potential becomes

$$V_{\text{eff}}(\sigma_c) = \frac{N}{2\lambda} \sigma_c^2 - 2N \int \frac{d^2 p}{(2\pi)^2} \sqrt{\mathbf{p}^2 + \sigma_c^2} . \quad (3.4)$$

The momentum integral in Eq. (3.4) is ultraviolet divergent. By using a momentum cutoff Λ to regulate the divergent term in $V_{\text{eff}}(\sigma_c)$, we can define a renormalization condition for the coupling as

$$\frac{1}{\lambda_R(m)} = \frac{1}{N} \left. \frac{d^2 V_{\text{eff}}(\sigma_c)}{d\sigma_c^2} \right|_{\sigma_c=m} , \quad (3.5)$$

where m is a regularization scale. Equation (3.5) gives (neglecting terms of $\mathcal{O}(1/\Lambda)$),

$$\frac{1}{\lambda_R(m)} = \frac{1}{\lambda} - \frac{\Lambda}{\pi} + \frac{2m}{\pi} . \quad (3.6)$$

Next, by defining a renormalization invariant coupling as [14]

$$\frac{1}{\lambda_R} = \frac{1}{\lambda_R(m)} - \frac{2m}{\pi} , \quad (3.7)$$

we obtain that in terms of λ_R the renormalized effective potential reads (after subtracting an irrelevant field-independent divergent vacuum term)

$$V_{\text{eff,R}}(\sigma_c) = \frac{N}{2\lambda_R} \sigma_c^2 + \frac{N}{3\pi} |\sigma_c|^3 . \quad (3.8)$$

The minimum $\bar{\sigma}_c$ of $V_{\text{eff,R}}(\sigma_c)$ is given by

$$\bar{\sigma}_c = \begin{cases} \sigma_0 , & \lambda_R < 0 , \\ 0 , & \lambda_R > 0 , \end{cases} \quad (3.9)$$

where $\sigma_0 = \pi/|\lambda_R|$. Thus, dynamical chiral symmetry breaking, in the absence of external fields, only occurs for a negative coupling constant.

Using (3.8) and performing the (finite) momentum integrals for the temperature- and chemical-potential-dependent terms in Eq. (3.3), the renormalized effective potential at finite T and μ becomes

$$\begin{aligned} V_{\text{eff}}(\sigma_c, T, \mu) &= V_{\text{eff,R}}(\sigma_c) \\ &+ \frac{N}{\pi} T^2 |\sigma_c| \left\{ \text{Li}_2[-e^{-\beta(\sigma_c - \mu)}] + \text{Li}_2[-e^{-\beta(\sigma_c + \mu)}] \right\} \\ &+ \frac{N}{\pi} T^3 \left\{ \text{Li}_3[-e^{-\beta(\sigma_c - \mu)}] + \text{Li}_3[-e^{-\beta(\sigma_c + \mu)}] \right\} , \end{aligned} \quad (3.10)$$

where $\text{Li}_\nu(z)$ is the polylogarithm function, and it is defined (for $\nu > 0$) as [15]

$$\text{Li}_\nu(z) = \sum_{k=1}^{\infty} \frac{z^k}{k^\nu}.$$

From Eq. (3.10), we can derive the gap equation, which is defined from

$$\left. \frac{\partial}{\partial \sigma_c} V_{\text{eff}}(\sigma_c, T, \mu) \right|_{\sigma_c = \bar{\sigma}_c(T, \mu)} = 0, \quad (3.11)$$

which gives

$$\bar{\sigma}_c = \bar{\sigma}_c(T=0, \mu=0) - \frac{1}{\beta} \left\{ \ln \left[1 + e^{-\beta(\bar{\sigma}_c + \mu)} \right] + \ln \left[1 + e^{-\beta(\bar{\sigma}_c - \mu)} \right] \right\}. \quad (3.12)$$

The behavior of $\bar{\sigma}_c$ is well known [9, 16]. At $T = 0$, there is a critical chemical potential μ_c at which the chiral symmetry is restored (we are considering the case here where chiral symmetry breaking happens, i.e., for $\lambda_R < 0$). This can be shown to happen through a first-order phase transition, defined by the relation $V_{\text{eff,R}}(\sigma_c = 0, \mu_c) = V_{\text{eff,R}}(\sigma_c = \sigma_0, \mu_c)$. This yields the critical chemical potential $\mu_c = \sigma_0$. Thus, at zero temperature, we have the ground state of the system given by

$$\bar{\sigma}_c = \begin{cases} \sigma_0, & \text{for } \mu < \mu_c, \\ 0, & \text{for } \mu \geq \mu_c. \end{cases} \quad (3.13)$$

At finite temperature and chemical potential, there is a critical curve $\bar{\sigma}_c(T, \mu) = 0$, which is obtained from Eq. (3.12). This gives a line of second-order phase transition in the (μ, T) plane, starting at the critical point $(\mu = 0, T = T_c)$, where $T_c = \sigma_0/(2 \ln 2)$, and ending in a first-order critical point at $(\mu = \mu_c, T = 0)$. Note that when going beyond the mean field approximation, this structure can slightly change [17], leading to a first-order critical line merging with the second-order critical line at a tricritical point. In this work, we will restrict our analysis at the mean field approximation only.

B. The effective potential for the GN model at finite T , μ and in a tilted magnetic field

Let us now investigate the effective potential for the system in the presence of a tilted magnetic field, with components (B_\parallel, B_\perp) . The effective potential can once again be derived from Eq. (2.5) and it can also follow directly from Eqs. (3.1) or (3.3). In the case where the magnetic field has only an in-plane component, $B_\parallel \neq 0$ and $B_\perp = 0$, we have a shift of the chemical potential and we need to distinguish in the effective potential, not only the contributions from particles and antiparticles, but also the contributions from particles with spin up and spin down, with chemical potentials $\mu_\uparrow = \mu + \delta\mu$ and $\mu_\downarrow = \mu - \delta\mu$, respectively, and with $B_\perp = 0$, $\delta\mu = g \mu_B B_\parallel / 2$. Throughout this work we will be considering μ and $\delta\mu$ as positive quantities. Equation (3.3) for the renormalized effective potential, in this case, becomes

$$\begin{aligned} V_{\text{eff}}(\sigma_c, T, \mu_\uparrow, \mu_\downarrow) &= \frac{N}{2\lambda_R} \sigma_c^2 + \frac{N}{3\pi} |\sigma_c|^3 \\ &- NT \int \frac{d^2 p}{(2\pi)^2} \left[\ln \left(1 + e^{-\beta E_\uparrow^+} \right) + \ln \left(1 + e^{-\beta E_\uparrow^-} \right) \right] \\ &- NT \int \frac{d^2 p}{(2\pi)^2} \left[\ln \left(1 + e^{-\beta E_\downarrow^+} \right) + \ln \left(1 + e^{-\beta E_\downarrow^-} \right) \right], \end{aligned} \quad (3.14)$$

where $E_{\uparrow,\downarrow}^\pm = E_p \pm |\mu_{\uparrow,\downarrow}|$. A detailed analysis of the phase structure in this case was performed in Ref. [8]. The main effect of the in-plane magnetic field is to further contribute towards chiral symmetry restoration. In this case, it can be shown that the chiral symmetry will remain always restored (at any T and μ) for a critical asymmetry $\delta\mu_c \geq \mu_c = \sigma_0$.

Finally, we can also include in the above equation (3.14) a perpendicular component for the magnetic field, $B_\perp \neq 0$, by properly accounting for the Landau energy levels and degeneracies. For instance, in Eq. (3.14), we can take [6, 7] $E_p = \sqrt{\mathbf{p}^2 + \sigma_c^2} \rightarrow \sqrt{2k|eB_\perp| + \sigma_c^2}$, $k = 0, 1, 2, \dots$, the momentum integrals are replaced by a sum over the Landau levels, with a density of states $|eB_\perp|/(2\pi)$ and by also accounting for the degeneracy of the $k \geq 1$ Landau levels, we obtain

$$\begin{aligned} \frac{1}{N} V_{\text{eff,R}}(\sigma_c, T, \mu, B_\perp, \delta\mu) = & \frac{\sigma_c^2}{2\lambda_R} - \frac{\sqrt{2}|eB_\perp|^{3/2}}{\pi} \zeta\left(-\frac{1}{2}, \frac{\sigma_c^2}{2|eB_\perp|} + 1\right) - \frac{|\sigma_c||eB_\perp|}{2\pi} \\ & - \frac{|eB_\perp|}{4\pi\beta} \left\{ \ln\left(1 + e^{-\beta(|\sigma_c| - \mu_\uparrow)}\right) + \ln\left(1 + e^{-\beta(|\sigma_c| + \mu_\uparrow)}\right) \right. \\ & + 2 \sum_{k=1}^{\infty} \ln\left(1 + e^{-\beta(\sqrt{\sigma_c^2 + 2k|eB_\perp|} - \mu_\uparrow)}\right) \\ & + 2 \sum_{k=1}^{\infty} \ln\left(1 + e^{-\beta(\sqrt{\sigma_c^2 + 2k|eB_\perp|} + \mu_\uparrow)}\right) \\ & \left. + (\mu_\uparrow \rightarrow |\mu_\downarrow|) \right\}, \end{aligned} \quad (3.15)$$

where $\zeta(s, a)$ is the Hurwitz zeta function [18],

$$\zeta(s, a) = \sum_{k=0}^{\infty} \frac{1}{(k+a)^s}. \quad (3.16)$$

Equation (3.15) can be seen as a generalization of the mean field theory (or large- N approximation) result derived, e.g., in Refs. [7, 14], for the case considered here, where we have a parallel component of the magnetic field (or equivalently, an asymmetry between the spin-up and spin-down components of the fermion field).

An important feature concerning the (2+1)-dimensional GN model in a magnetic field, when $B_\perp \neq 0$ and taking $B_\parallel = 0$, is that it can be shown that a nonvanishing global minimum can always develop for the effective potential, even when the coupling in Eq. (3.15) is positive. This is the phenomenon of *magnetic catalysis*, found and studied at length, e.g., in Refs. [6, 7]. The behavior for the global minimum $\bar{\sigma}_c$ for small values of B_\perp , at $B_\parallel = T = \mu = 0$, has been determined to be given by [6]

$$\bar{\sigma}_c = \begin{cases} \frac{1}{2\pi} |\lambda_R| |eB_\perp| + \dots, & \lambda_R > 0, \\ \sigma_0 \left[1 + \frac{|eB_\perp|^2}{12\sigma_0^4} + \dots \right], & \lambda_R < 0. \end{cases} \quad (3.17)$$

Thus, the component of the magnetic field perpendicular to the plane always tends to break (or enhance) the chiral symmetry. On the other hand, as we have already commented above, a parallel (in-plane) magnetic field component $B_\parallel \neq 0$ has been shown [8] to always tend to restore the chiral symmetry. Therefore, when both components of the magnetic field are present, one can expect that there must be a competing effect between the in-plane component B_\parallel and the perpendicular component B_\perp . While the former tends to suppress the chiral symmetry due to the increase of the magnitude of the Zeeman energy term (the asymmetry $\delta\mu$), the latter tends to enhance the chiral-symmetry-broken region. We then expect that the interplay of the two components of the magnetic field, when applied simultaneously and independently to the system, will possibly lead to a rich structure for the phase diagram. This indeed will be true, as we will show below. As we will show, the simultaneous and independent application of external magnetic fields in parallel and perpendicular to the system's plane can generate multicritical points and reentrant phases. These are results not seen in those cases when only one component of the magnetic field is present. It is quite surprising that such study of the simultaneous effect of both components of the magnetic field in the GN in 2+1 dimensions has not been done before, despite the fact that this is a kind of physical situation that has been of increasing interest in the context of experiments with planar types of condensed matter systems in the laboratory. We will comment more on this in the Conclusions section.

C. The phase diagram in the presence of a tilted magnetic field

We now turn to the study of the phase diagram for the (2+1)-dimensional GN model, with the effective potential given by Eq. (3.15). The equation for the gap $\bar{\sigma}_c$, which is determined from the equation defining the minimum of

the effective potential,

$$\left. \frac{d}{d\sigma_c} V_{\text{eff,R}}(\sigma_c, T, \mu, B_\perp, \delta\mu) \right|_{\sigma_c=\bar{\sigma}_c} = 0, \quad (3.18)$$

and that generalizes Eq. (3.12), becomes

$$\begin{aligned} 0 = & \frac{1}{\lambda_R} \bar{\sigma}_c - \frac{\sqrt{2}}{2\pi} |eB_\perp|^{\frac{1}{2}} \bar{\sigma}_c \zeta\left(\frac{1}{2}, \frac{\bar{\sigma}_c^2}{2|eB_\perp|}\right) + \frac{|eB_\perp|}{2\pi} \\ & + \frac{|eB_\perp|}{4\pi} \left\{ \frac{1}{e^{\beta(\bar{\sigma}_c - \mu_\uparrow)} + 1} + \frac{1}{e^{\beta(\bar{\sigma}_c + \mu_\uparrow)} + 1} \right. \\ & + 2\bar{\sigma}_c \sum_{k=1}^{\infty} \frac{1}{(\bar{\sigma}_c^2 + 2k|eB_\perp|)^{\frac{1}{2}}} \left[\frac{1}{e^{\beta(\sqrt{\bar{\sigma}_c^2 + 2k|eB_\perp|} - \mu_\uparrow)} + 1} \right. \\ & \left. \left. + \frac{1}{e^{\beta(\sqrt{\bar{\sigma}_c^2 + 2k|eB_\perp|} + \mu_\uparrow)} + 1} \right] + (\mu_\uparrow \rightarrow |\mu_\downarrow|) \right\}. \end{aligned} \quad (3.19)$$

A second-order phase transition critical point is found when, by changing any of the external parameters T , μ , B_\perp and/or the asymmetry $\delta\mu$, $\bar{\sigma}_c$ changes continuously and vanishes at the critical point. For a first-order phase transition, we have, instead, that $\bar{\sigma}_c$ is discontinuous at the critical point. We are interested in obtaining the critical points by varying a set of parameters, while others are kept fixed. For example, we can initially fix the values for the asymmetry and for the perpendicular to the plane component of the magnetic field, while varying the temperature and chemical potential. For fixed values of B_\perp and $\delta\mu$, a second-order transition line in the (μ, T) plane then follows from those critical points for which $\bar{\sigma}_c$ vanishes in a continuous way along this critical line. In a first-order transition, the effective potential develops different minima, $\bar{\sigma}_c^{(1)} \neq \bar{\sigma}_c^{(2)}$, where one of them is a local minimum, while the other is a global minimum. These minima can become degenerate for some values of the parameters. The first-order transition line is then determined by the condition of degeneracy of the minima of the effective potential,

$$V_{\text{eff,R}}(\bar{\sigma}_c^{(1)}, T_c, \mu_c, B_\perp, \delta\mu) = V_{\text{eff,R}}(\bar{\sigma}_c^{(2)}, T_c, \mu_c, B_\perp, \delta\mu). \quad (3.20)$$

In general, one of the minima is the trivial solution, $\bar{\sigma}_c = 0$, though this may not be always true, depending on the parameters chosen in Eq. (3.15), as we will verify explicitly below. In all cases, the critical lines are determined numerically, by solving the gap equation (3.19) and by also verifying the condition of Eq. (3.20). The point where the second-order critical line meets the first-order critical line defines a tricritical point in the phase diagram.

Let us initially show the effect on the phase structure of the system when only one of the components of the magnetic field is applied to the system, i.e., for the case of $\delta\mu \neq 0$, $B_\perp = 0$ (i.e., when only the parallel component of the magnetic field is present) and for the case when $\delta\mu = 0$, but $B_\perp \neq 0$ corresponding to the case of neglecting the Zeeman energy term, or, equivalently, when $B_\parallel = 0$ and the contribution of B_\perp through the Zeeman energy term is small enough such that it can be neglected (which is the case in most of the relevant physical situations, as discussed in Sec. II and exemplified in the Conclusions section). In Fig. 2 we show each of these cases in terms of the phase diagram in the (μ, T) plane. In the two plots shown in the figure, the external region to the curves is a chiral-symmetry-restored phase region, $\bar{\sigma}_c = 0$, while the internal region to the curves is a chiral-symmetry-broken phase region, $\bar{\sigma}_c \neq 0$. For simplicity, we are not showing the metastable regions that would appear around the first-order transition lines in the plot on the right. These metastable regions will be discussed and shown below. Figure 2(a) is for the case where the perpendicular component of the magnetic field is absent, $B_\perp = 0$. In this case, the critical lines for different values for the asymmetry $\delta\mu$ ($B_\parallel \neq 0$) are found to be all of second order. The only first-order transition point happens at $T = 0$ and $\mu_c = \sigma_0$. For a critical value of the asymmetry $\delta\mu_c = \sigma_0$, we find that $\bar{\sigma}_c = 0$ for any value of the temperature. Note that this critical value for the asymmetry has the same value as for μ_c , found in the absence of the Zeeman energy term [16]. This is a consequence of the symmetry between the Zeeman energy term ($\delta\mu$) and the chemical potential. Figure 2(b) is for the case where the in-plane component of the magnetic field is absent, $B_\parallel = 0$, but $B_\perp \neq 0$ (and its contribution to $\delta\mu$ is neglected). The structure obtained in this case is the one previously found in the earlier papers [6, 7], where, besides the second-order transition line, now a first-order transition line also appears, with a tricritical point between them. The effect due to magnetic catalysis is clear, showing that the larger B_\perp is, the larger the symmetry-broken region will be. It is then clear from the results

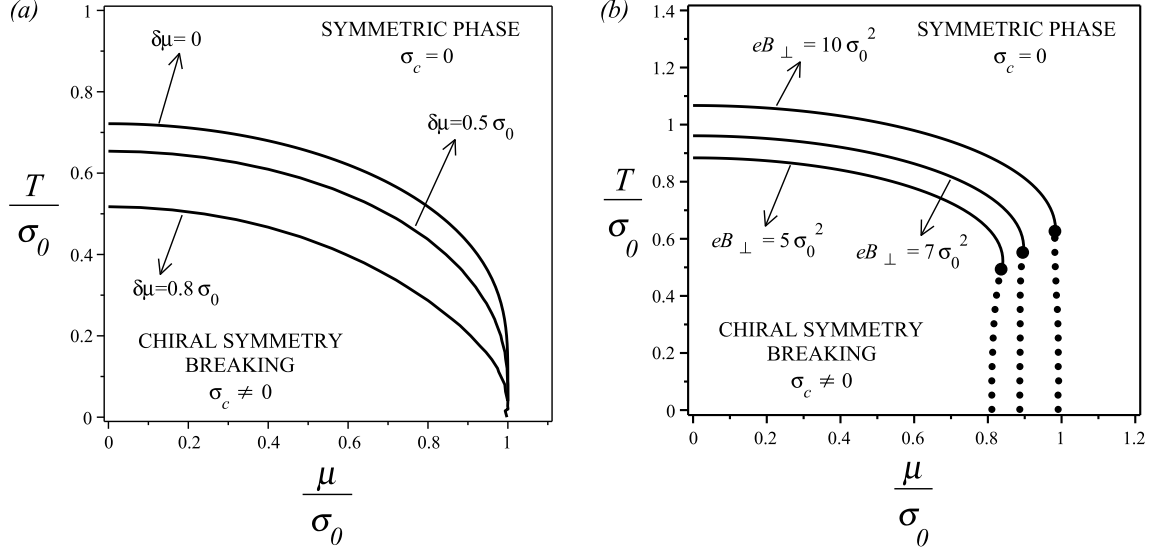


FIG. 2: The phase diagram in the (μ, T) plane for $\lambda_R < 0$. (a) The plot on the left shows the critical curves in the case of $B_\perp = 0$ and for different values of $\delta\mu$. (b) The plot on the right shows the critical curves for the case of $\delta\mu = 0$ (in the absence of a Zeeman energy term) and for different values of B_\perp . The solid lines are second-order critical lines and the dotted lines are first-order critical lines. The tricritical points are marked by the large dots in the plot on the right. All quantities are expressed in units of $\sigma_0 = \pi/|\lambda_R|$.

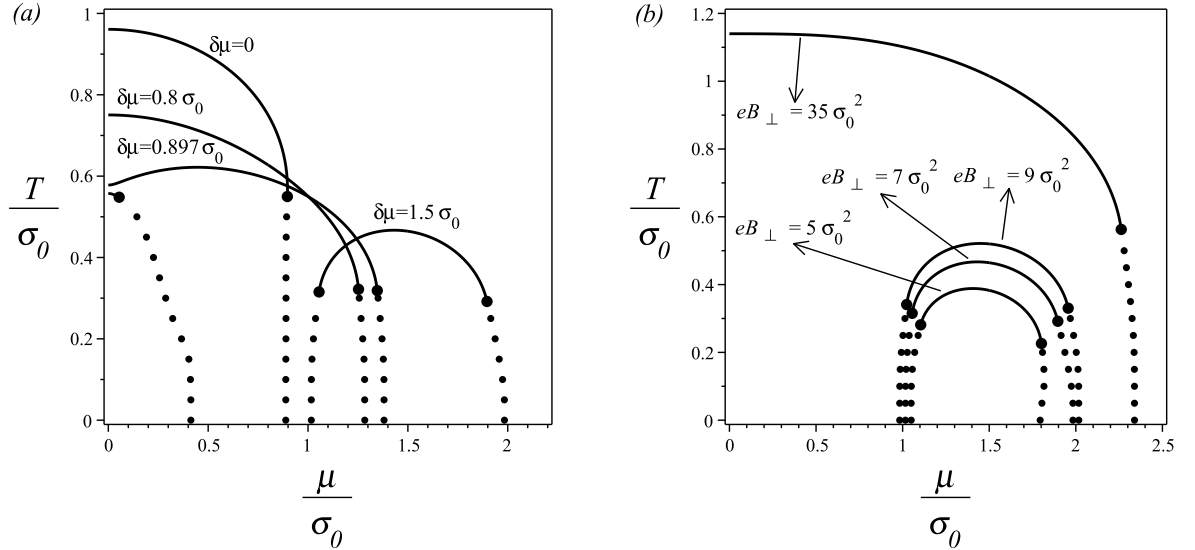


FIG. 3: The phase diagram in the (μ, T) -plane for $\lambda_R < 0$. (a) The plot on the left shows the critical curves in the case of fixed $|eB_\perp| = 7\sigma_0^2$ and for different values of $\delta\mu$. (b) The plot on the right shows the critical curves for the case of fixed $\delta\mu = 1.5\sigma_0$ and for different values of $|eB_\perp|$. The solid lines are second-order critical lines and the dotted lines are first-order critical lines. The tricritical points are marked by the large dots in the plots.

shown in Fig. 2 that the Zeeman energy term tends to act to restore the chiral symmetry, while the perpendicular magnetic field alone tends to enlarge the chiral-symmetry-broken region.

In Fig. 3 we show the effects of increasing either the asymmetry $\delta\mu$ or the perpendicular component of the magnetic field. In Fig. 3(a) the perpendicular magnetic field is kept constant at the value of $|eB_\perp| = 7\sigma_0^2$ and the asymmetry $\delta\mu$ is varied. In Fig. 3(b) we show the opposite case, where we keep fixed the asymmetry $\delta\mu$ at the value $\delta\mu = 1.5\sigma_0$, while the perpendicular component of the magnetic field is varied. A noticeable feature that we now observe in each of these cases, not seen in the previous figure, is the possibility of the emergence of multiple critical points and reentrant

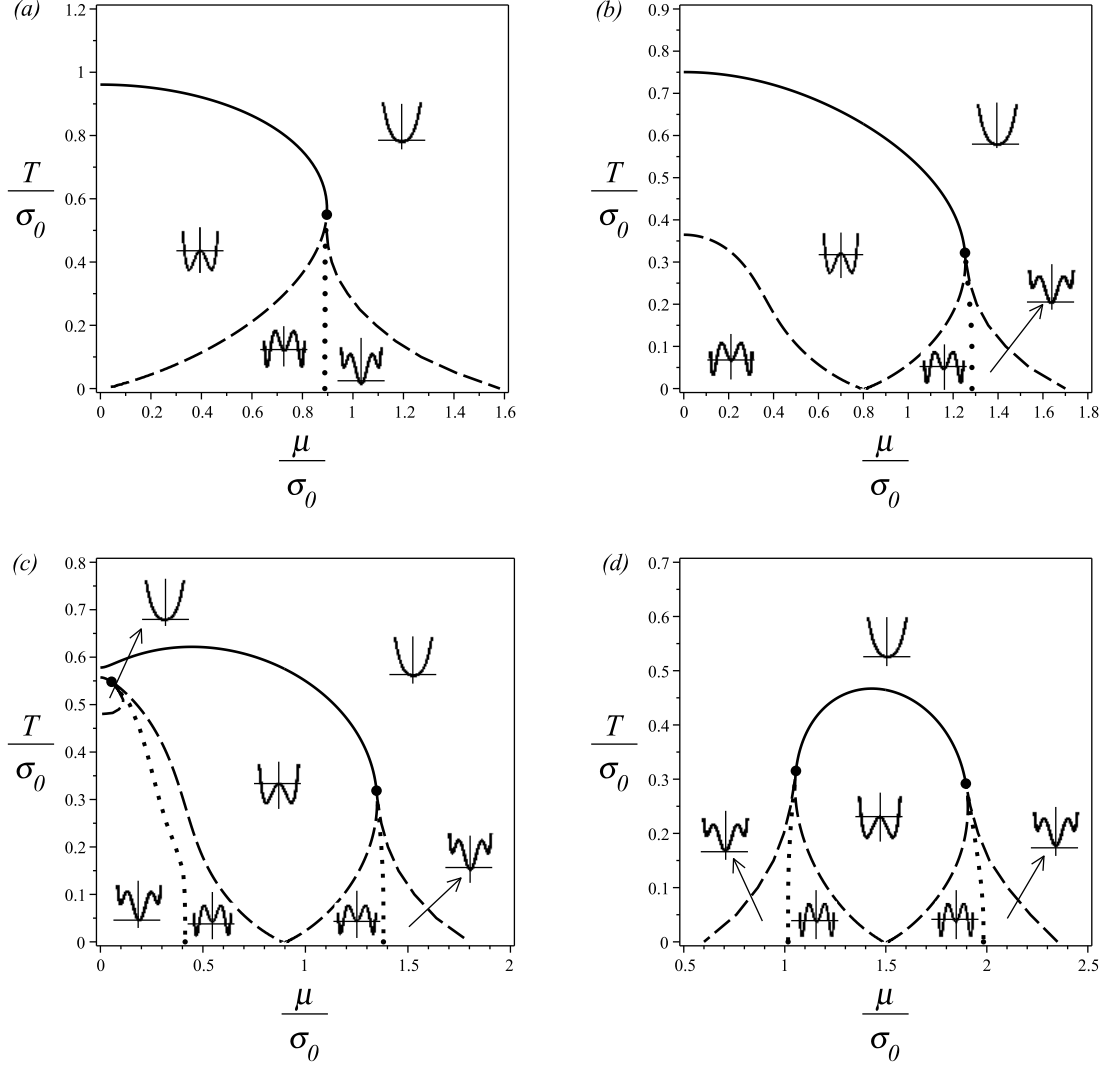


FIG. 4: The phase diagram (including the metastable lines) in the (μ, T) plane. The perpendicular magnetic field is fixed in $|eB_\perp| = 7\sigma_0^2$. The panel (a) on the top left shows the critical curves in the case of $\delta\mu = 0$. The panel (b) on the top right shows the critical curves for the case of $\delta\mu = 0.8\sigma_0$. The panel (c) on the bottom left shows the critical curves for the case of $\delta\mu = 0.897\sigma_0$. The panel (d) on the bottom right shows the critical curves for the case of $\delta\mu = 1.5\sigma_0$. The solid lines are second-order critical lines, the dotted lines are first-order critical lines and the dashed lines are the metastable critical lines. The tricritical points are marked by the large dots in the plots. Also shown is the schematic shape of the effective potential in each region of the phase diagram.

phases. In the case of fixed B_\perp , Fig. 3(a), after some critical value for the asymmetry, which for the parameters taken for this plot is $\delta\mu \simeq 0.895\sigma_0$, a second tricritical point emerges with an associated first-order transition line. In the plot shown in Fig. 3(b), we have purposively considered a value of asymmetry of $\delta\mu = 1.5\sigma_0$. Recall that for an asymmetry above the critical value of $\delta\mu_c = \sigma_0$ and $B_\perp = 0$, the chiral symmetry would always be restored [8]. However, as we start increasing B_\perp , a symmetry-broken region starts to emerge after some large enough value for the perpendicular magnetic field. This region of chiral-symmetry-broken phase that appears also has the form of the multicritical curves shown in Fig. 3(a). For a sufficiently large value of B_\perp , which for the parameters used in the plot of Fig. 3(b) is $|eB_\perp| \simeq 35\sigma_0^2$, one of the additional tricritical points (and its associated first-order transition line) disappears and the phase diagram shows again a standard form with a second-order critical line, a first-order transition line and a tricritical point in between them, a structure just like the ones shown in Fig. 2(b). The combined effect of both the Zeeman energy term, generating the asymmetry, and the perpendicular component of the magnetic field, producing the Landau energy levels and associated magnetic catalysis, is able to lead to reentrant phase transitions, as seen from the results in Fig. 3, whenever more than one tricritical point is present. This feature will be even more apparent

when we consider the zero-temperature limit and look at the possibility of quantum phase transitions at fixed values of B_\perp and $\delta\mu$ and varying chemical potential, a situation we will analyze in more detail below, in Sec. IV.

For completeness, in Fig. 4 we present the detailed structure for some of the phase diagrams shown in Fig. 3, including now the metastable lines. The metastable lines give the points for which a local minimum of the effective potential first appears or disappears. These lines are the ones shown on the left and on the right of the first-order critical lines. Again, from the results shown in Figs. 4(c) and 4(d), we can see the presence of reentrant phase transitions at some fixed temperature and varying chemical potential (e.g., the analogue of varying the doping in condensed matter systems). Reentrant phase transitions are always associated with more than one critical point. Multiple critical points can appear with more frequency as we decrease the temperature and, in particular, as we enter the quantum regime ($T = 0$). In the next section we will analyze this situation more carefully.

IV. QUANTUM PHASE TRANSITION PATTERNS

In order to better understand the reentrant phases found in the previous section, it is convenient to first look at those cases where $T = 0$, i.e., for the quantum regime. Taking the $T = 0$ limit in Eq. (3.15), we obtain

$$\begin{aligned} \frac{1}{N} V_{\text{eff,R}}(\sigma_c, T, \mu, B_\perp, \delta\mu) &\xrightarrow{T \rightarrow 0} \frac{\sigma_c^2}{2\lambda_R} - \frac{\sqrt{2}|eB_\perp|^{3/2}}{\pi} \zeta\left(-\frac{1}{2}, \frac{\sigma_c^2}{2|eB_\perp|} + 1\right) - \frac{|\sigma_c||eB_\perp|}{2\pi} \\ &- \frac{|eB_\perp|}{4\pi} \left[(\mu_\uparrow - |\sigma_c|) \theta(\mu_\uparrow - |\sigma_c|) + (|\mu_\downarrow| - |\sigma_c|) \theta(|\mu_\downarrow| - |\sigma_c|) \right. \\ &+ 2 \sum_{k=1}^{k_{\max}^\uparrow} \left(\mu_\uparrow - \sqrt{2k|eB_\perp| + \sigma_c^2} \right) \theta(\mu_\uparrow^2 - \sigma_c^2) \\ &\left. + 2 \sum_{k=1}^{k_{\max}^\downarrow} \left(|\mu_\downarrow| - \sqrt{2k|eB_\perp| + \sigma_c^2} \right) \theta(\mu_\downarrow^2 - \sigma_c^2) \right], \end{aligned} \quad (4.1)$$

where

$$k_{\max}^{\uparrow,\downarrow} = \text{Int} \left(\frac{\mu_{\uparrow,\downarrow}^2 - \sigma_c^2}{2|eB_\perp|} \right), \quad (4.2)$$

and $\text{Int}(x)$ means the integer part of x .

We can now look at the phase diagram in the $(\mu, \delta\mu)$ plane at fixed B_\perp . An example is shown in Fig. 5. Note from Fig. 5 that for fixed values for the asymmetry $\delta\mu$, we can find multiple reentrant phases. Examples of how these reentrant phases manifest from the effective potential are shown in Fig. 6 for two specific values of asymmetry, $\delta\mu = 0.7\sigma_0$ and $\delta\mu = 0.9\sigma_0$.

From the forms of the effective potential shown in Fig. 6, we see that two forms of (first-order) reentrant phase transitions are possible for the asymmetry and when the chemical potential is increased. We can have a reentrant phase transition starting at a chiral broken state, $\bar{\sigma}_c = \sigma_1$, going to one or more intermediate chiral broken states with $\bar{\sigma}_c = \sigma_2$, $\sigma_1 > \sigma_2$, and then to a chiral symmetric state, $\bar{\sigma}_c = 0$. This is the case shown, e.g., in the first panel in Fig. 6. The other possibility is, starting from a chiral symmetric state, $\bar{\sigma}_c = 0$, going to one or more intermediate chiral broken states, with $\bar{\sigma}_c \neq 0$, and then back to the chiral symmetric state. This is, e.g., represented in the second panel in Fig. 6.

A. Quantum phase transitions in the fully polarized system

It is interesting to notice from Fig. 5 that the reentrant phases are maximal (occur more frequently) when $\mu = \delta\mu$. This corresponds to the full polarization regime, $\mu_\uparrow = 2\mu$ and $\mu_\downarrow = 0$. In Fig. 7 we show the values assumed for the vacuum expectation value $\bar{\sigma}_c$ along this full polarization regime. By increasing the chemical potential, the value of $\bar{\sigma}_c$ can decrease discontinuously through many intermediate first-order phase transitions. This type of pattern is found to be exclusive of the full polarization regime.

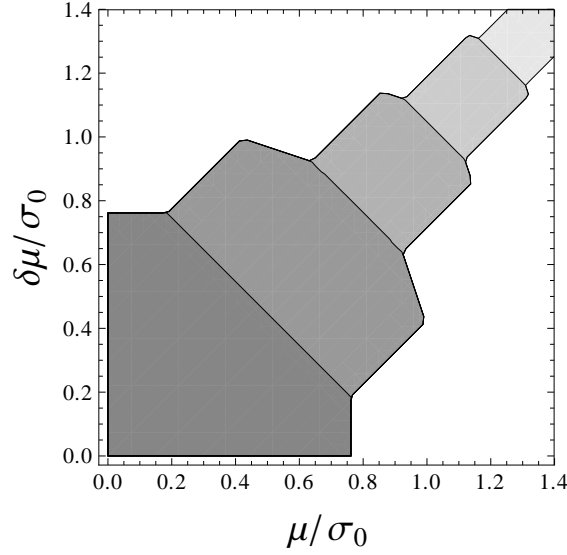


FIG. 5: The phase diagram in the $(\mu, \delta\mu)$ plane and at $T = 0$. The perpendicular magnetic field component was fixed at the value of $|eB_\perp| = \sigma_0^2$. The different shadows of gray indicate decreasing values for the vacuum expectation value $\bar{\sigma}_c$. Going from dark to light shadows, we have $\bar{\sigma}_c/\sigma_0 \simeq 1.0617, 0.8144, 0.3669, 0.2883$. Outside the shadowed areas, $\bar{\sigma}_c = 0$. All solid lines indicate first-order phase transition lines.

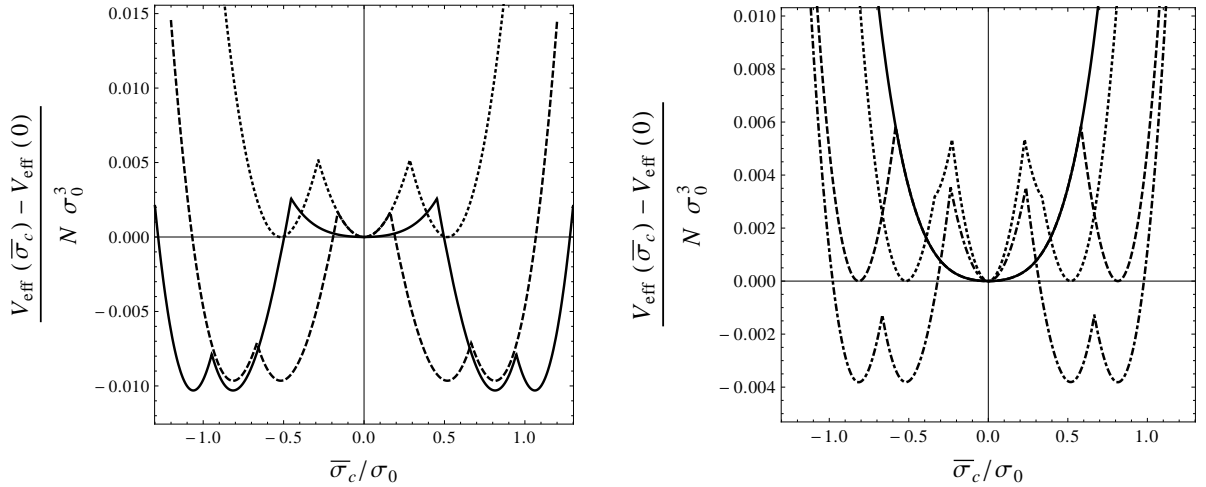


FIG. 6: The effective potential for a fixed value of $|eB_\perp| = \sigma_0^2$ and for different values of chemical potential μ and asymmetry $\delta\mu$. The plot on the left is for $\delta\mu = 0.7\sigma_0$ and for $\mu/\sigma_0 \simeq 0.2467$ (solid curve), $\mu/\sigma_0 \simeq 0.8633$ (dashed curve) and $\mu/\sigma_0 \simeq 0.9845$ (dotted curve). For $\mu/\sigma_0 > 0.9845$, there is only one global minimum at $\bar{\sigma}_c = 0$ and chiral symmetry is restored. The plot on the right is for $\delta\mu = 0.9\sigma_0$ and for $\mu/\sigma_0 = 0$ (solid curve), $\mu/\sigma_0 \simeq 0.3172$ (dashed curve), $\mu/\sigma_0 \simeq 0.6633$ (dash-dotted curve) and $\mu/\sigma_0 \simeq 1.1282$ (dotted curve). For $\mu/\sigma_0 < 0.3172$ and for $\mu/\sigma_0 > 1.1282$, there is only one global minimum at $\bar{\sigma}_c = 0$ and chiral symmetry is restored.

Though this pattern of multiple phase transitions can happen at any nonzero value of B_\perp in principle, this structure is not stable when thermal fluctuations are accounted for. Upon leaving the quantum regime $T = 0$ and by increasing the temperature, the intermediate transitions going from a value of $\bar{\sigma}_c = \sigma_1$ to a value σ_2 (where $\sigma_1 > \sigma_2$) quickly disappear. This can be easily understood from the results shown for the effective potential in Fig. 6. These intermediate first-order transitions are in general characterized by a small potential barrier. By increasing the temperature, these intermediate minima in the potential are quickly smoothed out. The smaller B_\perp is, the smaller the temperature needed to smooth out the intermediate transitions will be. For example, in Fig. 8, we have the case of $|eB_\perp| = \sigma_0^2$ and for a temperature of $T = 0.06\sigma_0$, which are taken as representative values. All intermediate transitions are smoothed out and $\bar{\sigma}_c$ becomes mostly a continuously varying function, with only the strongest first-order transition remaining, which the first one shown in Fig. 7, which also remains in Fig. 8. By further increasing the temperature, the transition

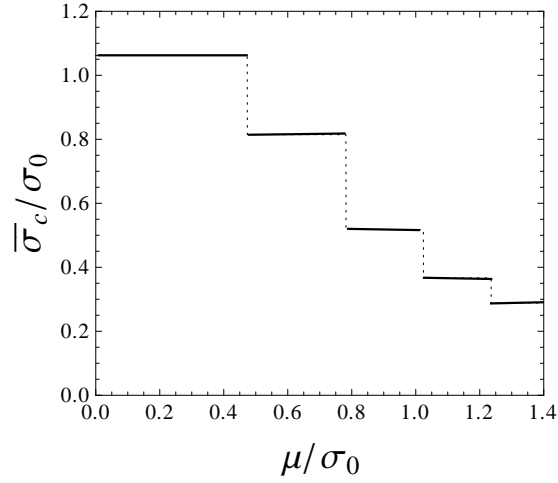


FIG. 7: The values assumed for the vacuum expectation value $\bar{\sigma}_c$ along the line $\delta\mu = \mu$ in Fig. 5.

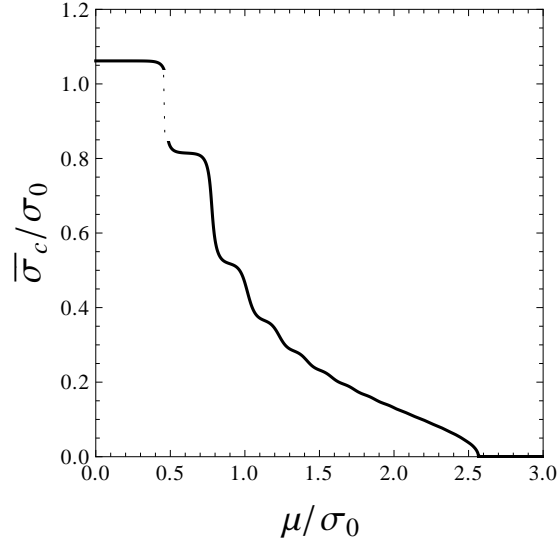


FIG. 8: The values assumed for the vacuum expectation value $\bar{\sigma}_c$ along the line $\delta\mu = \mu$, when $|eB_\perp| = \sigma_0^2$ and $T = 0.06\sigma_0$.

becomes just a second-order one, with $\bar{\sigma}_c$ continuously varying before vanishing completely at a given critical value of chemical potential. This corresponds to crossing one of the lines of second-order phase transition.

From the expression for the effective potential in the $T = 0$ limit, Eq. (4.1), we can find approximate analytical expressions for the vacuum expectation value $\bar{\sigma}_c$ in the large magnetic field regime, with $|eB_\perp| \gg \mu^2$ and $|eB_\perp| \gg \bar{\sigma}_c^2$. For instance, in the $\mu = \delta\mu = 0$ case, we find, valid for either positive or negative values of λ_R ,

$$\bar{\sigma}_c(T = 0, \delta\mu = 0, \mu = 0) \simeq \frac{\lambda_R |eB_\perp|}{2\pi - \sqrt{2|eB_\perp|} \zeta(1/2) \lambda_R}, \quad (4.3)$$

where $\zeta(1/2) \simeq -1.46035$, while for the case when there is only the perpendicular component of the magnetic field, with $B_\parallel = 0$ and setting $\delta\mu = 0$, we find

$$\bar{\sigma}_c(T = 0, \delta\mu = 0, \mu) \simeq \begin{cases} \frac{\lambda_R |eB_\perp|}{2\pi - \sqrt{2|eB_\perp|} \zeta(1/2) \lambda_R}, & \mu < \tilde{\mu}_c, \\ 0, & \mu \geq \tilde{\mu}_c, \end{cases} \quad (4.4)$$

where

$$\tilde{\mu}_c \simeq \frac{\lambda_R |eB_\perp|}{4\pi - 2\sqrt{2|eB_\perp|}\zeta(1/2)\lambda_R} . \quad (4.5)$$

These results can be compared with the one in the fully polarized case, $\delta\mu = \mu \neq 0$. Taking $|eB_\perp| \gg \mu^2$ and $\mu \gg \bar{\sigma}_c$, we find

$$\bar{\sigma}_c(T=0, \delta\mu = \mu) \simeq \frac{\lambda_R |eB_\perp|}{4\pi - 2\sqrt{2|eB_\perp|}\zeta(1/2)\lambda_R} , \quad (4.6)$$

which is half of the value obtained for $\bar{\sigma}_c$ when $\mu = \delta\mu = 0$, Eq. (4.3).

B. Hall conductivity

It is not only convenient but also useful to look at possible physical quantities that can be measured in the laboratory and give confirmation of the existence of the reentrant and multiple phase transitions we have found above. In most realistic experiments, the measured quantities of interest are related, for example, to susceptibilities, like the magnetic susceptibility and also quantities related to electric transport. In the presence of a tilted magnetic field, we can have each field contributing differently to these quantities. For example, it is expected that the enhancement of the Zeeman splitting caused by the in-plane component of the magnetic field will have important effects in the experiments with graphene and also with other planar systems. Based on experimental studies of an in-plane magnetic field in graphene, the Zeeman splitting has been shown to be important in both the spin transport and conductance fluctuation properties [19]. It has also been shown that the Zeeman splitting leads to the spectrum of the effective single-particle Hamiltonian exactly as required by the observed pattern of quantization of Hall conductivity [20]. Since the Hall conductivity is a typical quantity of importance for analysis when studying these systems, we will here concentrate on the possible effects the reentrant and multiple phase transitions we have found can have on it.

The Hall conductivity, σ_H , can be defined as [10]

$$\sigma_H = \frac{e^2}{|eB_\perp|} n , \quad (4.7)$$

where n is the number density,

$$n = -\frac{\partial}{\partial\mu} V_{\text{eff,R}}(\sigma_c, T, \mu, B_\perp, \delta\mu) \Big|_{\sigma_c = \bar{\sigma}_c} . \quad (4.8)$$

From the zero-temperature limit for the effective potential, Eq. (4.1), we find

$$\begin{aligned} \sigma_H(\bar{\sigma}_c, T=0, \mu, B_\perp, \delta\mu) &= \frac{Ne^2}{4\pi} \left[1 + 2 \text{Int} \left(\frac{\mu_\uparrow^2 - \bar{\sigma}_c^2}{2|eB_\perp|} \right) \right] \theta(\mu_\uparrow - |\bar{\sigma}_c|) \\ &+ \frac{Ne^2}{4\pi} \text{sign}(\mu_\downarrow) \left[1 + 2 \text{Int} \left(\frac{\mu_\downarrow^2 - \bar{\sigma}_c^2}{2|eB_\perp|} \right) \right] \theta(|\mu_\downarrow| - |\bar{\sigma}_c|) , \end{aligned} \quad (4.9)$$

where $\text{sign}(x)$ is the sign function.

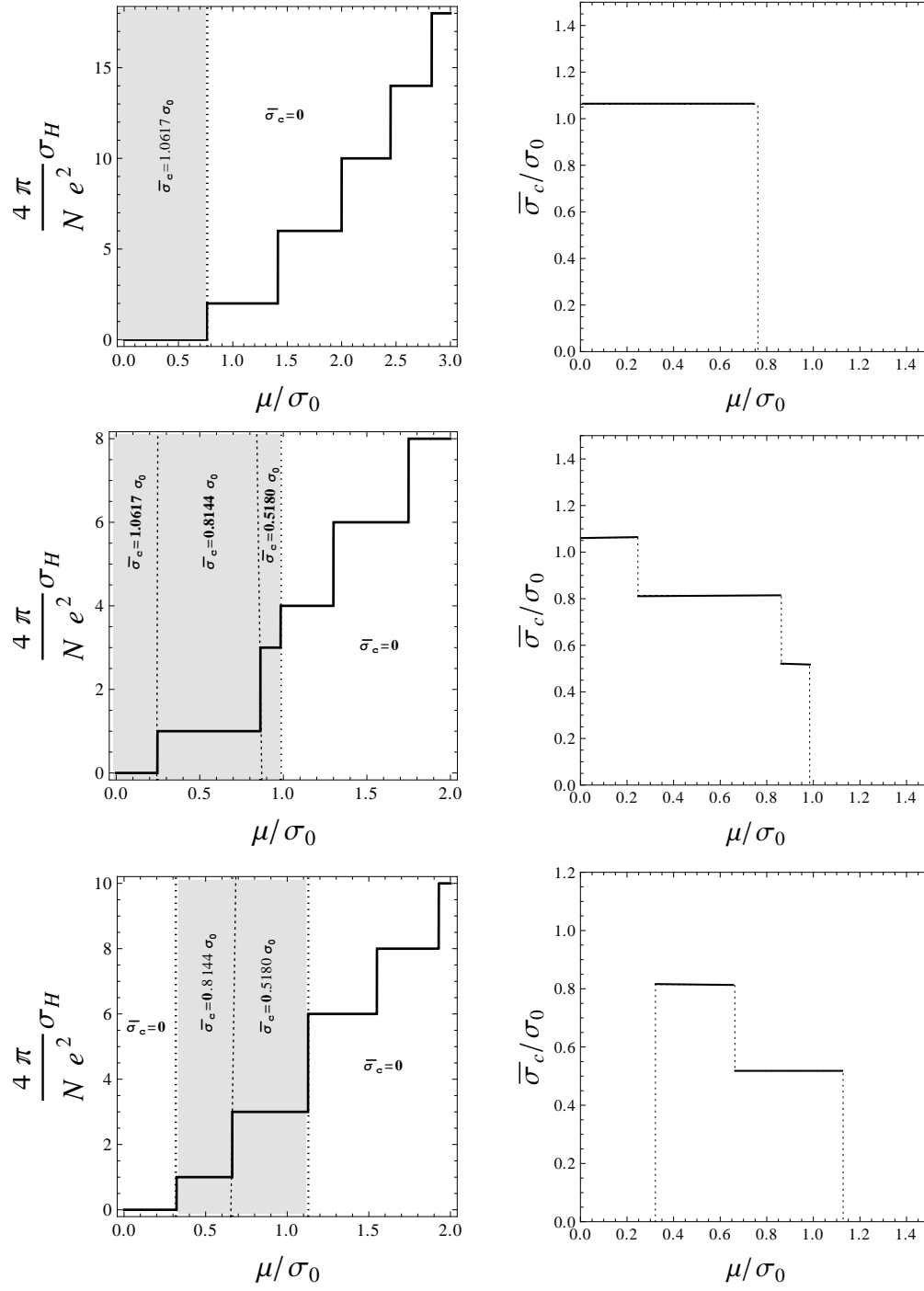


FIG. 9: The Hall conductivity, at zero temperature, as a function of chemical potential (plots on the left). The vertical thin dotted lines separate the regions for which $\bar{\sigma}_c$ changes value (discontinuously). The plots on the right show the corresponding variation of $\bar{\sigma}_c$ with the chemical potential. From top to bottom we have the cases of $\delta\mu = 0$, $\delta\mu = 0.7\sigma_0$ and $\delta\mu = 0.9\sigma_0$. The perpendicular component of the magnetic field is held fixed at the value $|eB_\perp| = \sigma_0^2$.

In Fig. 9 we show some representative cases for the Hall conductivity at $T = 0$, as a function of the chemical potential and for different values for the asymmetry $\delta\mu$. We have again kept fixed, for convenience, the perpendicular component of the magnetic field in the value $|eB_\perp| = \sigma_0^2$ as a representative example. The vertical dotted lines in the plots on the left indicate the positions of the phase transitions, with the shaded areas indicating the chiral-symmetry-breaking regions and the corresponding values assumed for $\bar{\sigma}_c$. The pattern of chiral phase transition in each case is shown in the plots on the right. Note that each time there is a transition, the Hall conductivity can jump by a different factor than in the absence of chiral symmetry breaking. As the chemical potential is increased from zero,

the largest differences appear at the first transition and at the last transition, when the system enters in the chiral symmetric region. This behavior is quite different from that seen when computing the Hall conductivity in quantum electrodynamics (see, e.g., Ref. [21]) where there are no gaps and transitions, i.e., where $\bar{\sigma}_c = 0$. The presence of a gap $\bar{\sigma}_c$ and its capacity to change as the chemical potential is changed, as seen in the previous subsection, is responsible for the differences in the Hall conductivity. This is determined by the relations between $\mu_{\uparrow, \downarrow}$ and $\bar{\sigma}_c$, for a given value of B_{\perp} , as can be inferred from Eq. (4.9). Recalling that $\mu_{\uparrow} = \mu + \delta\mu$ and $\mu_{\downarrow} = \mu - \delta\mu$, we find for the Hall conductivity the following behaviors as we vary the values of μ and $\delta\mu$:

- When $\mu_{\downarrow} \geq 0$:

$$\begin{aligned} \frac{4\pi}{Ne^2} \sigma_H(\bar{\sigma}_c, T=0, \mu, B_{\perp}, \delta\mu) &= \left[1 + 2 \operatorname{Int} \left(\frac{\mu_{\uparrow}^2 - \bar{\sigma}_c^2}{2|eB_{\perp}|} \right) \right] \theta(\mu_{\uparrow} - |\bar{\sigma}_c|) \\ &+ \left[1 + 2 \operatorname{Int} \left(\frac{\mu_{\downarrow}^2 - \bar{\sigma}_c^2}{2|eB_{\perp}|} \right) \right] \theta(|\mu_{\downarrow}| - |\bar{\sigma}_c|) . \end{aligned} \quad (4.10)$$

- If $|\mu_{\downarrow}| > |\bar{\sigma}_c|$, we always have that $\mu_{\uparrow} > |\bar{\sigma}_c|$ and

$$\frac{4\pi}{Ne^2} \sigma_H(\bar{\sigma}_c, T=0, \mu, B_{\perp}, \delta\mu) = 2 \left[1 + \operatorname{Int} \left(\frac{\mu_{\uparrow}^2 - \bar{\sigma}_c^2}{2|eB_{\perp}|} \right) + \operatorname{Int} \left(\frac{\mu_{\downarrow}^2 - \bar{\sigma}_c^2}{2|eB_{\perp}|} \right) \right] . \quad (4.11)$$

- If $\mu_{\uparrow} > |\bar{\sigma}_c|$ and $|\mu_{\downarrow}| < |\bar{\sigma}_c|$, then

$$\frac{4\pi}{Ne^2} \sigma_H(\bar{\sigma}_c, T=0, \mu, B_{\perp}, \delta\mu) = 1 + \operatorname{Int} \left(\frac{\mu_{\uparrow}^2 - \bar{\sigma}_c^2}{2|eB_{\perp}|} \right) . \quad (4.12)$$

- If $\mu_{\uparrow} < |\bar{\sigma}_c|$, we always have that $|\mu_{\downarrow}| < |\bar{\sigma}_c|$, then

$$\frac{4\pi}{Ne^2} \sigma_H(\bar{\sigma}_c, T=0, \mu, B_{\perp}, \delta\mu) = 0 . \quad (4.13)$$

- When $\mu_{\downarrow} < 0$:

$$\begin{aligned} \frac{4\pi}{Ne^2} \sigma_H(\bar{\sigma}_c, T=0, \mu, B_{\perp}, \delta\mu) &= \left[1 + 2 \operatorname{Int} \left(\frac{\mu_{\uparrow}^2 - \bar{\sigma}_c^2}{2|eB_{\perp}|} \right) \right] \theta(\mu_{\uparrow} - |\bar{\sigma}_c|) \\ &- \left[1 + 2 \operatorname{Int} \left(\frac{\mu_{\downarrow}^2 - \bar{\sigma}_c^2}{2|eB_{\perp}|} \right) \right] \theta(|\mu_{\downarrow}| - |\bar{\sigma}_c|) . \end{aligned} \quad (4.14)$$

- If $|\mu_{\downarrow}| > |\bar{\sigma}_c|$, we always have that $\mu_{\uparrow} > |\bar{\sigma}_c|$, then:

$$\frac{4\pi}{Ne^2} \sigma_H(\bar{\sigma}_c, T=0, \mu, B_{\perp}, \delta\mu) = 2 \left[\operatorname{Int} \left(\frac{\mu_{\uparrow}^2 - \bar{\sigma}_c^2}{2|eB_{\perp}|} \right) - \operatorname{Int} \left(\frac{\mu_{\downarrow}^2 - \bar{\sigma}_c^2}{2|eB_{\perp}|} \right) \right] . \quad (4.15)$$

- If $\mu_{\uparrow} > |\bar{\sigma}_c|$ and $|\mu_{\downarrow}| < |\bar{\sigma}_c|$, we have that:

$$\frac{4\pi}{Ne^2} \sigma_H(\bar{\sigma}_c, T=0, \mu, B_{\perp}, \delta\mu) = 1 + \operatorname{Int} \left(\frac{\mu_{\uparrow}^2 - \bar{\sigma}_c^2}{2|eB_{\perp}|} \right) . \quad (4.16)$$

– If $\mu_{\uparrow} < |\bar{\sigma}_c|$, we always have that $|\mu_{\downarrow}| < |\bar{\sigma}_c|$ and

$$\frac{4\pi}{Ne^2}\sigma_H(\bar{\sigma}_c, T=0, \mu, B_{\perp}, \delta\mu) = 0. \quad (4.17)$$

Equations (4.16) and (4.17) are identical to Eqs. (4.12) and (4.13), respectively (the sign of μ_{\downarrow} does not interfere in these cases). Thus, we have four distinct possibilities for the Hall conductivity, given by Eqs. (4.11), (4.12), (4.15) and (4.17).

We also note that by accounting for the effect of thermal fluctuations, we will have two effects on the Hall conductivity. First, as seen in the previous subsection, it will tend to smooth out the intermediate transitions and only the strongest first-order phase transitions tend to remain at a given temperature. Second, including the effect of temperature, the Hall conductivity itself is smoothed out. This is shown in Fig. 10, for the example of asymmetry $\delta\mu = 0.9\sigma_0$ that was considered in Fig. 9. Note that for the values of temperature considered, the intermediate transition disappears and only the first and last transitions remain, the one entering the chiral-symmetry-broken region and the one leaving it, respectively.

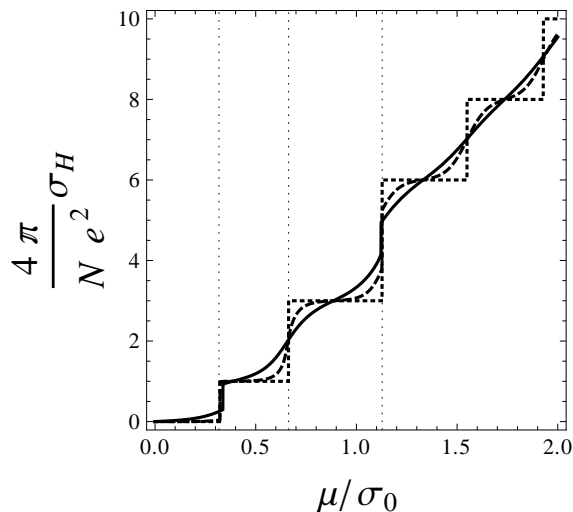


FIG. 10: The Hall conductivity for $|eB_{\perp}| = \sigma_0^2$, $\delta\mu = 0.9\sigma_0$ and for $T = 0$ (dotted line), $T = 0.05\sigma_0$ (dashed line) and $T = 0.1\sigma_0$ (solid line).

V. CONCLUSIONS

In this work we have studied how an external tilted magnetic field, with nonvanishing components parallel and perpendicular to the system's plane, can affect the phase diagram for planar fermions in a GN type of model with discrete chiral symmetry. Though in this work we have concentrated on the transition patterns found for the chiral fermionic condensate, we can easily extend our work to include also a superconducting gap [22]. We will investigate this in detail elsewhere.

As far the chiral symmetry is concerned, the parallel component of the magnetic field leads to a Zeeman effect in these planar systems that tends to weaken the chiral symmetry. Thus, the chiral symmetry phase transition, which in condensed matter systems can be associated with an insulating-to-metal type of transition, may happen at a smaller critical temperature in the presence of a Zeeman field. This behavior, due to an increasing magnetic Zeeman field, is exactly the opposite of that observed when a perpendicular magnetic field is applied to the system (see e.g. Refs. [6, 7]). In a perpendicular magnetic field the chiral symmetry breaking becomes stronger as a consequence of the effect of the magnetic field, a behavior associated with the magnetic catalysis in the system. (Note that magnetic catalysis is not an effect exclusive to fermionic systems but can also occur in bosonic systems as well [23], enlarging the symmetry-broken region in those systems). Thus, in the presence of a perpendicular magnetic field the transition happens at a higher critical temperature. We have shown that this competing effect of each component of the external magnetic field applied to the system can produce a rich phase diagram, with the production of multiple critical points and reentrant phase transitions.

Note that there are many systems that can display multiple phase transitions, most particularly in low-energy condensed matter systems, where they can be found more easily. At the quantum field theory level, reentrant phases have been shown to be possible in systems with coupled scalar fields in the nonrelativistic limit [24]. Multiple phase transitions can in principle also be found in relativistic systems. This can be the case, for example, in systems with two or more coupled scalar fields (see, for example, Ref. [25] and references therein). Multiple critical points in effective models for quantum chromodynamics have also been shown to be possible in Ref. [26]. However, to our knowledge, no reentrant phase transitions of the type we have found here have been shown before to appear in fermionic relativistic systems.

As a way to determine the presence of multiple critical points and reentrant phase transitions, we have computed the Hall conductivity. We have seen that whenever a first-order phase transition happens, the Hall conductivity jumps by a different amount at the critical point. This is a consequence of the different value assumed (discontinuously) for the chiral vacuum expectation value $\bar{\sigma}_c$, as analyzed in Sec. IV B. Since the Hall conductivity σ_H is an important measurable quantity for diverse condensed matter systems, like for semiconductor materials, superconductor films and graphene, our results indicate a way that the presence of a gap in the system and quantum phase transitions may reflect on the measurements of σ_H .

It is tempting to try to directly apply our results to the physics of graphene, for instance. In these systems we can have both components of the magnetic field acting concomitantly. However, in most studies (see, e.g., Ref. [27]) the Zeeman energy term (which for us here is given by the asymmetry term $\delta\mu$) is much smaller than the energy splitting between Landau levels. This is easily understood if we use typical values found in realistic planar condensed matter systems, including, for example, graphene. Recall that the Zeeman energy is $\delta\mu = g\mu_B B/2$, where B is the total magnitude of the magnetic field. Using $g = 2$, $\mu_B = e/(2m_e)$, where $m_e = 0.511$ MeV is the electron rest mass, $e \simeq 1/\sqrt{137}$ and the conversion factor 1 Tesla $\simeq 692.4$ eV², we find, by expressing B in terms of the perpendicular component of the field and the tilt angle ϕ (see Fig. 1), that

$$\delta\mu \simeq 0.058 \frac{B_{\perp}[\text{T}]}{\sin \phi} \text{ meV}, \quad (5.1)$$

where $B[\text{T}]$ is the absolute value of the magnetic field in units of teslas. For the Landau energy level splitting between the zeroth and first levels, we find that

$$E_{LL} = \sqrt{2v_F^2 |eB_{\perp}|} \simeq 36.3 \sqrt{B_{\perp}[\text{T}]} \text{ meV}, \quad (5.2)$$

where we have reestablished the Fermi velocity in the above expression and used that $v_F \sim c/300$ (e.g., like for graphene). We then find for the ratio $\delta\mu/E_{LL} \simeq 0.0016 \sqrt{B_{\perp}[\text{T}]} / \sin \phi$. The Zeeman energy term $\delta\mu$ is then comparable to E_{LL} only for extremely large values of the magnetic field (e.g., for $B_{\perp} \gtrsim 3.9 \times 10^5$ Teslas, when taking for instance that $B_{\parallel} = 0$), or for a highly tilted magnetic field, such that $\sin \phi \ll 1$. For typical laboratory magnetic fields of $\mathcal{O}(10)$ Teslas or for a not-too-much tilted magnetic field (such that $B_{\perp} \gtrsim B_{\parallel}$), we find that $\delta\mu \ll E_{LL}$. So, indeed, under these circumstances, the Zeeman energy term becomes negligible and also justifies neglecting it when $B_{\parallel} = 0$.

For the type of phenomena we have found in this paper, we can already find reentrant and multiple phase transitions for asymmetries as small as $\delta\mu \sim 0.1\sigma_0$ and at a temperature $T \lesssim 0.01\sigma_0$. Taking a perpendicular component for the magnetic field of $v_F^2 |eB_{\perp}| \sim 10\sigma_0^2$ (where we have reestablished again the Fermi velocity in the expression for the Landau energy levels, as appropriate for fermionic condensed matter systems) and for a typical gap energy σ_0 of around 10 meV [28], we find $T \lesssim 1$ K and a required field with $B_{\perp} \sim 1.5$ Teslas and, upon using Eq. (5.1), we obtain $\sin \phi \sim 0.087$, which then gives $B_{\parallel} \sim 17.2$ Teslas. This corresponds to a highly tilted magnetic field in the direction of the system's plane, which is the expected physical situation where the effects of the Zeeman energy term start to become important and cannot be neglected, according to the estimates shown above (for these values of parameters, the Zeeman energy term $\delta\mu$ is about 2.3% of the value of E_{LL}). These estimates for the required values of magnetic fields seem reasonable and low enough to be achieved in the laboratory and this does not seem such a highly special situation to be produced in practice. Besides, with the increasing precision being reached in the most recent experiments, it may be possible to realize such an experiment with superconductor films under these tuned conditions and probe the type of transitions we have found in this paper, for example through the measurements of the Hall conductivity, as we have suggested.

In conclusion, we have seen that the opposite effects caused by magnetic fields, when applied parallel and perpendicular to the system's plane, can lead to a rich pattern of phase transitions. The results we have found here can have immediate applications in the context of the physics of planar condensed matter systems, including graphene, planar films of conducting polyacetylene and high-temperature superconductor films. In all these systems, the viability of their application as modern semiconductor devices is directly related to the ability of producing and controlling a

gap. Our results indicate that this control can be achieved through an appropriate doping of the system and under parallel and perpendicular magnetic fields, that are applied simultaneously and independently, when properly tuned. If these conditions can be achieved, then our results can open interesting possibilities for the uses of these type of materials in practical applications as novel electronic devices.

Acknowledgments

The authors thank K. G. Klimenko for useful comments and suggestions. R.O.R. is partially supported by research grants from Conselho Nacional de Desenvolvimento Científico e Tecnológico (CNPq) and Fundação Carlos Chagas Filho de Amparo à Pesquisa do Estado do Rio de Janeiro (FAPERJ). P.H.A.M. is supported by Coordenação de Aperfeiçoamento de Pessoal de Nível Superior (CAPES).

-
- [1] D. V. Khveshchenko, Phys. Rev. Lett. **87**, 206401 (2001); E. V. Gorbar, V. P. Gusynin, V. A. Miransky and I. A. Shovkovy, Phys. Rev. B **66**, 045108 (2002); H. Leal and D. V. Khveshchenko, Nucl. Phys. B **687**, 323 (2004).
 - [2] V. P. Gusynin and S. G. Sharapov, Phys. Rev. Lett. **95**, 146801 (2005); V. P. Gusynin, V. A. Miransky, S. G. Sharapov and I. A. Shovkovy, Phys. Rev. B **74**, 195429 (2006).
 - [3] G. W. Semenoff, I. A. Shovkovy and L. C. R. Wijewardhana, Mod. Phys. Lett. A **13**, 1143 (1998); K. Krishana, N. P. Ong, Y. Zhang, *et. al.*, Phys. Rev. Lett. **82**, 5108 (1999); D. V. Khveshchenko, W. F. Shively, Phys. Rev. B **73**, 115104 (2006).
 - [4] K. S. Novoselov, *et. al.*, Nature **438**, 197 (2005).
 - [5] D. Gross and A. Neveu, Phys. Rev. D **10**, 3235 (1974).
 - [6] K. G. Klimenko, Theor. Math. Phys. **90**, 1 (1992) [Teor. Mat. Fiz. **90**, 3 (1992)]; Z. Phys. C **54**, 323 (1992); Theor. Math. Phys. **89**, 1161 (1992) [Teor. Mat. Fiz. **89**, 211 (1991)].
 - [7] V. P. Gusynin, V. A. Miransky and I. A. Shovkovy, Phys. Rev. Lett. **73**, 3499 (1994) [Erratum-ibid. **76**, 1005 (1996)] [hep-ph/9405262]; Phys. Rev. D **52**, 4718 (1995) [hep-th/9407168].
 - [8] H. Caldas and R. O. Ramos, Phys. Rev. B **80**, 115428 (2009).
 - [9] B. Rosenstein, B. Warr, and S. H. Park, Phys. Rept. **205**, 59 (1991).
 - [10] C. Kittel, *Introduction to Solid State Physics*, sixth ed., John Wiley & Sons, New York, (1986).
 - [11] J. I. Kapusta and C. Gale, *Finite-Temperature Field Theory: Principles and Applications*, (Cambridge University Press, Cambridge, England, 2006).
 - [12] S. Coleman, *Aspects of Symmetry* (Cambridge University Press, Cambridge, 1985).
 - [13] M. Moshe and J. Zinn-Justin, Phys. Rept. **385**, 69 (2003) [hep-th/0306133].
 - [14] A. S. Vshivtsev, K. G. Klimenko and B. V. Magnitsky, Theor. Math. Phys. **106**, 319 (1996) [Teor. Mat. Fiz. **106**, 390 (1996)].
 - [15] Handbook of Mathematical Functions, edited by M. Abramowitz and I. A. Steigen, Dover, 9th edition 1972.
 - [16] K. G. Klimenko, Z. Phys. C **37**, 457 (1988); B. Rosenstein, B. J. Warr and S. H. Park, Phys. Rev. D **39**, 3088 (1989); Phys. Rev. Lett. **62**, 1433 (1989).
 - [17] J. -L. Kneur, M. B. Pinto, R. O. Ramos and E. Staudt, Phys. Rev. D **76**, 045020 (2007) [arXiv:0705.0676 [hep-th]]; Phys. Lett. B **657**, 136 (2007) [arXiv:0705.0673 [hep-ph]].
 - [18] E. Elizalde, A. D. Odintsov and A. Romeo, *Zeta Regularization Techniques with Applications*, (River Edge, NJ, World Scientific, 1994).
 - [19] M. B. Lundeberg and J. A. Folk, Nature Physics **5**, 894 (2009).
 - [20] Y. Zhang, Z. Jiang, J. P. Small, M. S. Purewal, Y.-W. Tan, M. Fazlollahi, J. D. Chudow, J. A. Jaszczak, H. L. Stormer and P. Kim, Phys. Rev. Lett. **96**, 136806 (2006); Z. Jiang, Y. Zhang, Y.-W. Tan, H. L. Stormer and P. Kim, Solid State Commun. **143**, 14 (2007).
 - [21] A. Perez Martinez, E. Rodriguez Querts, H. Perez Rojas, R. Gaitan and S. Rodriguez-Romo, J. Phys. A **44**, 445002 (2011) [arXiv:1106.5722 [cond-mat.mes-hall]].
 - [22] K. G. Klimenko, R. N. Zhokhov and V. C. Zhukovsky, Phys. Rev. D **86**, 105010 (2012) [arXiv:1210.7934 [hep-th]]; arXiv:1211.0148 [hep-th].
 - [23] D. C. Duarte, R. L. S. Farias and R. O. Ramos, Phys. Rev. D **84**, 083525 (2011) [arXiv:1108.4428 [hep-ph]].
 - [24] M. B. Pinto, R. O. Ramos and J. E. Parreira, Phys. Rev. D **71**, 123519 (2005) [hep-th/0506131]; R. O. Ramos and M. B. Pinto, J. Phys. A **39**, 6687 (2006) [hep-th/0605259].
 - [25] M. B. Pinto and R. O. Ramos, Phys. Rev. D **61**, 125016 (2000) [hep-ph/9912273]; M. B. Pinto and R. O. Ramos, J. Phys. A **39**, 6649 (2006) [cond-mat/0605508].
 - [26] L. Ferroni, V. Koch and M. B. Pinto, Phys. Rev. C **82**, 055205 (2010) [arXiv:1007.4721 [nucl-th]].
 - [27] P. K. Pyatkovskiy and V. P. Gusynin, Phys. Rev. B **83**, 075422 (2011).
 - [28] S. Cho, N. P. Butch, J. Paglione and M. S. Fuhrer, Nano Lett. **11**, 1925 (2011); A. A. Taskin, S. Sasaki, K. Segawa and Y. Ando, Phys. Rev. Lett. **109**, 066803 (2012).